KURENAI 紅

Kyoto University Research Information Repository

KYOTO UNIVERSITY

Title	Development of a dual phantom technique for measuring the fast neutron component of dose in boron neutron capture therapy.
Author(s)	Sakurai, Yoshinori; Tanaka, Hiroki; Kondo, Natsuko; Kinashi, Yuko; Suzuki, Minoru; Masunaga, Shinichiro; Ono, Koji; Maruhashi, Akira
Citation	Medical physics (2015), 42(11): 6651-6657
Issue Date	2015-10-25
URL	http://hdl.handle.net/2433/203069
Right	© 2015 American Association of Physicists in Medicine; This is the accepted manuscrip of the article is available at http://dx.doi.org/10.1118/1.4934243; The full-text file will be made open to the public on 23 October 2016 in accordance with publisher's 'Terms and Conditions for Self-Archiving'.
Type	Journal Article
Textversion	author

Development of a dual phantom technique for measuring the fast neutron component of dose in boron neutron capture therapy

Yoshinori Sakurai, Hiroki Tanaka, Natsuko Kondo, Yuko Kinashi, Minoru Suzuki,

5   **Shinichiro Masunaga, Koji Ono, and Akira Maruhashi**

Kyoto University Research Reactor Institute, Asashironishi 2-1010, Kumatori-cho, Sennan-gun, Osaka 590-0494, Japan

Abstract

10   **Purpose:** Research and development of various accelerator-based irradiation systems for boron neutron capture therapy (BNCT) is underway throughout the world. Many of these systems are nearing or have started clinical trials. Before the start of treatment with BNCT, the relative biological effectiveness (RBE) for the fast neutrons (over 10 keV) incident to the irradiation field must be estimated. Measurements of RBE are typically performed by biological experiments with a

15   phantom. Although the dose deposition due to secondary gamma rays is dominant, the relative contributions of thermal neutrons (below 0.5 eV) and fast neutrons are virtually equivalent under typical irradiation conditions in a water and/or acrylic phantom. Uniform contributions to the dose deposited from thermal and fast neutrons is based in part on relatively inaccurate dose information for fast neutrons. This study sought to improve the accuracy in the dose estimation for fast neutrons

20   by using two phantoms made of different materials, in which the dose components can be separated according to differences in the interaction cross-sections. The development of a "dual phantom technique" for measuring the fast neutron component of dose is reported.

Methods: One phantom was filled with pure water. The other phantom was filled with a water solution of lithium hydroxide (LiOH) capitalizing on the absorbing characteristics of lithium-6 (Li-

25   6) for thermal neutrons. Monte Carlo simulations were used to determine the ideal mixing ratio of Li-6 in LiOH solution. Changes in the depth dose distributions for each respective dose component

along the central beam axis were used to assess the LiOH concentration at the 0, 0.001, 0.01, 0.1, 1 and 10 weight percent levels. Simulations were also performed with the phantom filled with 10 weight percent ^{6}LiOH solution for 95%-enriched Li-6. A phantom was constructed containing 10 weight percent ^{6}LiOH solution based on the simulation results. Experimental characterization of the depth dose distributions of the neutron and gamma-ray components along the central axis was performed at Heavy Water Neutron Irradiation Facility installed at Kyoto University Reactor using activation foils and thermo-luminescent dosimeters, respectively.

Results: Simulation results demonstrated that the absorbing effect for thermal neutrons occurred when the LiOH concentration was over 1%. The most effective Li-6 concentration was determined to be enriched ^{6}LiOH with a solubility approaching its upper limit. Experiments confirmed that the thermal neutron flux and secondary gamma-ray dose rate decreased substantially however the fast neutron flux and primary gamma-ray dose rate were hardly affected in the 10%-^{6}LiOH phantom. It was confirmed that the dose contribution of fast neutrons is improved from approximately 10% in the pure water phantom, to approximately 50% in the 10%-^{6}LiOH phantom.

Conclusions: The dual phantom technique using the combination of a pure water phantom and a 10%-^{6}LiOH phantom developed in this work provides an effective method for dose estimation of the fast neutron component in BNCT. Improvement in the accuracy achieved with the proposed technique results in improved RBE estimation for biological experiments and clinical practice.

Keywords: boron neutron capture therapy; fast neutron; dual phantom technique; lithium hydroxide; enriched lithium-6

I. INTRODUCTION

The first clinical study of boron neutron capture therapy (BNCT) at Kyoto University Research Reactor Institute (KURRI) was carried out in 1974.[1] Since then, Heavy Water Neutron Irradiation Facility (HWNIF) installed at Kyoto University Reactor (KUR) has been used for BNCT for

various types of tumors including malignant brain and head and neck tumors.[2] Operation of KUR was suspended in February 2006 for a fuel change from high-enriched uranium to low-enriched uranium.[3] Operations resumed in May 2010, including clinical BNCT irradiations. After restarting operation, 235 clinical BNCT irradiations have been performed at HWNIF as of September 2015.

In early 2009, a cyclotron-based system for clinical BNCT, known as the "Cyclotron-Based Epi-thermal Neutron Source (C-BENS)" was installed at KURRI.[4] The world's first accelerator-based BNCT was carried out for a brain tumor using this system in November 2012 and clinical trials for treatments using C-BENS are on-going as of September 2015. Currently, BNCT is performed at KURRI using the reactor-based and accelerator-based systems. Each system has unique irradiation characteristics which need to be understood and accounted for during clinical use.

Research and development into several types of accelerator-based irradiation systems is underway.[5-8] In the near future, BNCT using these newly developed irradiation systems may be carried out at multiple facilities across the world.[9]

It is important that the physical and biological estimations for dose quantity and quality are performed consistently among several irradiation fields, and that the equivalency of BNCT is guaranteed, within and across BNCT systems. In theory, the various different BNCT irradiation systems should provide similar neutron irradiation fields as they were designed according to the similar criteria for irradiation characteristics.[10] However, the neutron energy spectra vary among systems. Specifically, the mixing ratio of the fast neutron component (>10 keV) to the thermal and/or epi-thermal neutron components (<10 keV) varies between systems and must be characterized before clinical use.

The relative biological effectiveness (RBE) for neutrons is dependent on the energy. With this in mind, it is necessary that the RBE for fast neutrons incident to a new BNCT irradiation field be estimated by biological experiment, typically through a phantom study prior to clinical use. However, in a typical water and/or acrylic phantom, thermal neutrons (<0.5 eV) are generated in the phantom at almost the same level as fast neutrons. Moreover, secondary gamma rays are generated

in the phantom, and dominate the dose deposition under typical irradiation conditions. Subtraction

80 of the contributions to the dose from the secondary gamma rays and thermal neutrons is required to

estimate the RBE for fast neutrons, which increases the uncertainty in dose determination.

This study seeks to improve the accuracy in the dose measurement for fast neutrons through the

combination of phantoms made of different materials in which the dose components can be

separated according to differences in the interaction cross-sections. One phantom was filled with

85 pure water. The other phantom was filled with a water solution of lithium hydroxide (LiOH),

capitalizing on the absorbing characteristics of lithium-6 (Li-6) for thermal neutrons.[11]

In the same manner as boron-10 (B-10), Li-6 has a large (n,α) reaction cross-section with low-

energy neutrons. The reaction cross-section is large (940 barn for thermal neutrons), and no gamma

rays are generated in this reaction. Considering these characteristics, the neutron energy spectrum

90 can be hardened using a phantom containing a proper quantity of Li-6. As a result, it was expected

that the dose rates for thermal neutrons and secondary gamma rays would decrease substantially

without changing the dose distribution for fast neutrons. The combination of a pure water phantom

and a phantom containing Li-6 may result in a more accurate dose measurement for fast neutrons.

The development of a "dual phantom technique" for measuring the fast neutron component of

95 dose incident to BNCT irradiation fields is reported.

II. MATERIALS AND METHODS

II.A. Monte Carlo simulation

Lithium-6 is thought to be a suitable thermal neutron absorbent due to its large reaction cross-

100 section for thermal neutrons and lack of gamma-ray production. Water, acrylic resin, or

polyethylene are typical candidates for the base material of a phantom. However, lithium is an

alkali metal and does not readily mix with any of these base materials. Furthermore, it may ignite as

a result of a reaction with water. Therefore, it was necessary to select compounds containing lithium

as the base material for the phantom. A water solution of lithium hydroxide (LiOH) was chosen as

105   the phantom material which allowed for the mixing ratio of Li-6 to be regulated and the physical

characteristics could be well defined.

    As expected, a small mixing ratio of Li-6 in solution with LiOH decreases the thermal neutron

absorption, while a large mixing ratio substantially influences the dose distribution for fast

neutrons. Prior to construction of the phantom, the Li-6 mixing ratio was surveyed using MCNP-

110   4C.[12] Simulations were performed for LiOH concentrations of 0, 0.001, 0.01, 0.1, 1, and 10 in

weight percent. It should be noted that the upper limit of the solubility of the LiOH concentration in

water is 12–13 in weight percent at normal temperature. The LiOH concentrations studied

corresponded to Li-6 concentrations of 0, 0.26, 2.6, 26, 260 and 2,600 ppm, respectively, as the

natural abundance of Li-6 is 7.5%. Additional simulations were performed for a phantom with a

115   ^{6}LiOH solution of 10 weight percent, assuming that 95%-enriched Li-6 was used. For this phantom,
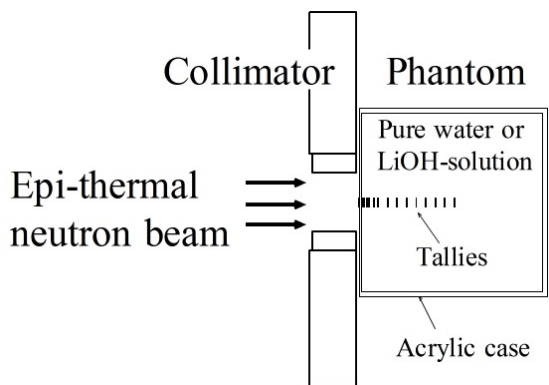
the Li-6 concentration corresponded to 25,000 ppm.

Figure 1 Schematic of simulation geometry.

120   Simulations were performed corresponding to the epi-thermal neutron irradiation mode of KUR-

HWNIF,[2] which is used in the on-going BNCT clinical study. Figure 1 shows a schematic of the

simulation geometry. This geometry corresponds to a typical model for BNCT for brain tumors.

The phantom was a cylindrical acrylic case filled with pure water or LiOH solution, with an outer

diameter of 20 cm and height of 20 cm. The walls of the phantom were 5 mm thick. The top

125   (irradiated) and bottom surfaces were 2 mm thick. The collimator was polyethylene with LiF. The

LiF in the collimator was 50 weight percent using the natural abundance of Li. The simulation

geometry included the collimator and phantom. The irradiation room walls and other system components were not explicitly modeled in this study.

Simulations were performed assuming the KUR power was 1 MW with an irradiation aperture 12 cm in diameter, corresponding to the experimental setup as described below. Changes in the depth-dose distributions of the thermal neutron flux, fast neutron flux, primary gamma-ray dose rate, and secondary gamma-ray dose rate along the central axis were considered.
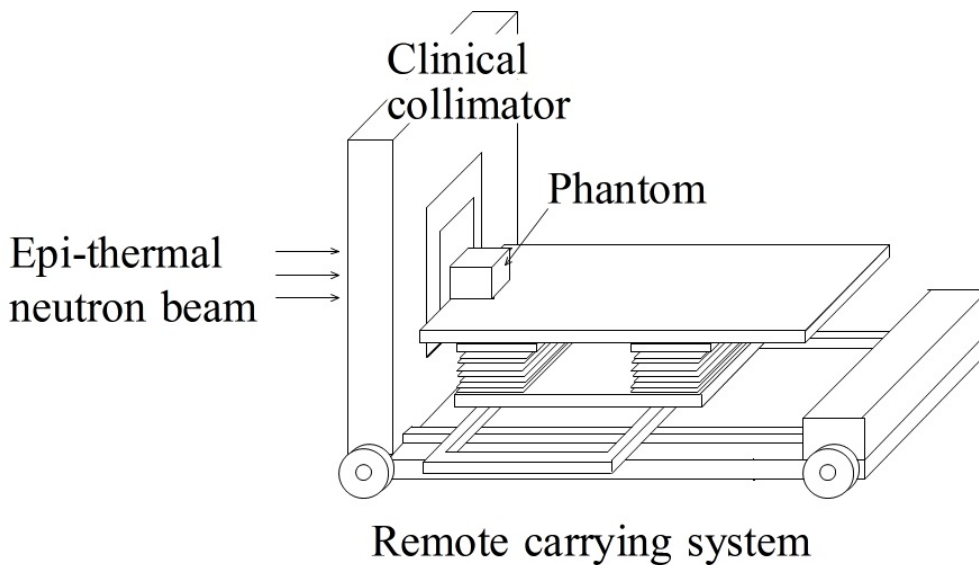
II.B. Experimental measurements

A ^{6}LiOH solution phantom of 10 weight percent was constructed based on the simulation results showing this concentration as the most effective for the enhancement of the fast neutron component. Figure 2 shows a schematic of the experimental setup. The phantom dimensions were the same as the simulation geometry. The epi-thermal neutron irradiation mode of KUR-HWNIF was used to irradiate the phantom, filled with either the ^{6}LiOH solution or pure water. The depth dose distributions of neutron flux and gamma-ray dose rate on the central axis were measured for each experimental setup.

The thermal neutron flux was measured with a gold wire 0.25 mm in diameter and cadmium pipe of 1 mm inner diameter and 2 mm outer diameter. For the measurement of fast neutron flux, an indium foil 10 mm in diameter and 127 μm thick was used. This foil was selected because of the relatively low energy threshold energy of the ^{115}In(n,n')^{115m}In reaction. A cadmium cover was used to reduce background and activation of thermal neutrons. The obtained saturated-activities for gold and indium were converted to thermal neutron flux and fast neutron flux (integrated in the energy range of 10 keV to 15 MeV), using the effective reaction cross-sections. The effective cross-section for each measurement point was calculated using the neutron energy spectrum determined from the simulation results.

Thermo-luminescent dosimeters (TLD) of beryllium oxide (BeO) were used for the measurement of gamma-ray dose rates. Commercially available BeO TLDs come in powder form, encapsulated

6

in borosilicate glass. These dosimeters have a high sensitivity to low-energy neutrons, specifically to thermal neutrons from the neutron irradiation fields of HWNIF, mainly due to the (n,α) reaction of B-10 in the borosilicate glass. Due to this intrinsic characteristic, BeO TLDs encapsulated with quartz glass (which does not contain B-10) were special ordered and used for measurements. Incidentally, BeO is also sensitive to low-energy neutrons. The thermal neutron fluence of 8×10^{12} cm^{-2} is approximately equal to 1 cGy of gamma-ray dose. The TLDs were used in conjunction with the gold foil to correct for the neutron sensitivity.

Figure 2 Schematic of experimental setup.

Considering the irradiation time necessary for accurate measurements, two irradiations were performed for each phantom. The first irradiation included the bare gold wire and TLD, and the second included the cadmium-covered gold wire and indium foil. The KUR power was 1 MW, and the irradiation time was 1 h for the former combination and 10 h for the latter combination. For reference, the KUR is operated at or below 1 MW for experiments to save fuel after the fuel low-enrichment process was completed. The KUR is only operated at 5 MW for clinical BNCT irradiations, which is the same power as used before the fuel low-enrichment.

III. RESULTS

III.A. Monte Carlo simulation

The simulation results for the depth distributions of the thermal neutron flux on the central axis in phantom are shown in Figure 3. Distributions are shown for the pure water phantom of 0%-LiOH concentration, the 1%-LiOH phantom, the 10%-LiOH phantom, and the 10%-^{6}LiOH phantom. The statistical errors are contained within the data marks, and the maximum error is 0.6% at the 10 cm depth for the 10%-^{6}LiOH phantom.

The distributions for the 0.001%-LiOH phantom, the 0.01%-LiOH phantom, and the 0.1%-LiOH phantom are not shown in Figure 3, as those results were essentially the same as those of the pure water phantom. When the LiOH concentration is over 1%, the absorbing effect for thermal neutrons becomes apparent. Compared with the pure water phantom, the thermal neutron flux decreased to 73% for the 1%-LiOH phantom and 22% for the 10%-LiOH phantom, at the 2 cm depth near the distribution peak. For the 10%-^{6}LiOH phantom, the thermal neutron flux was approximately 2% and decreased to almost one-fiftieth that at the 2 cm depth as compared with the pure water phantom.
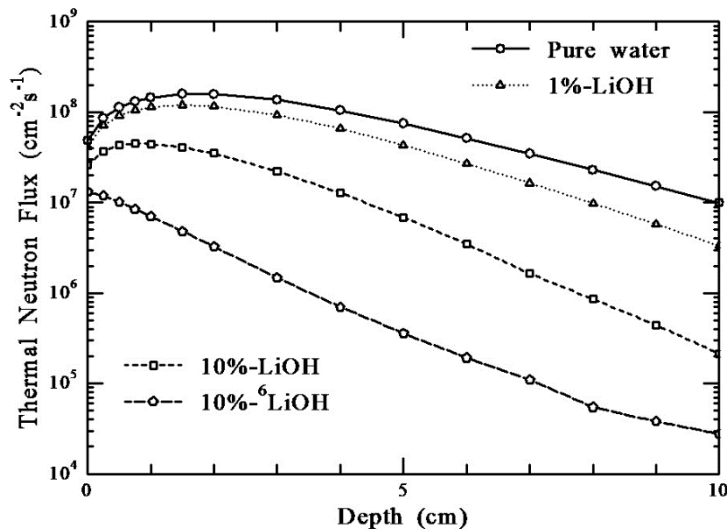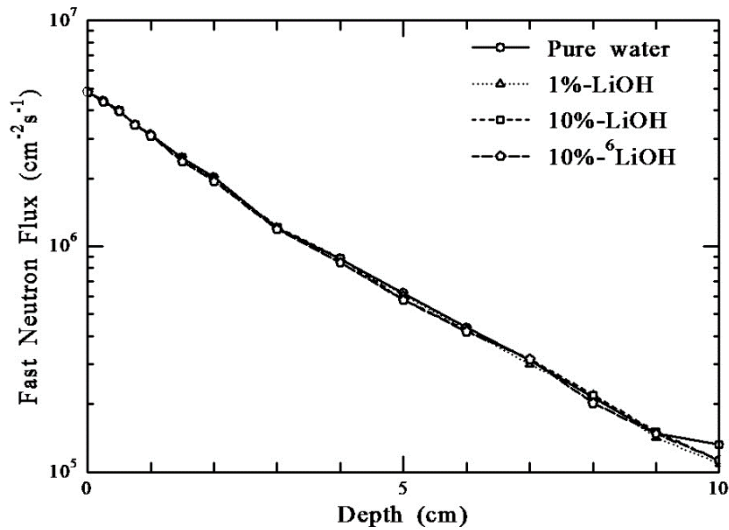

Figure 3 Simulation results for the depth distributions of the thermal neutron flux on the central axis in the phantoms.
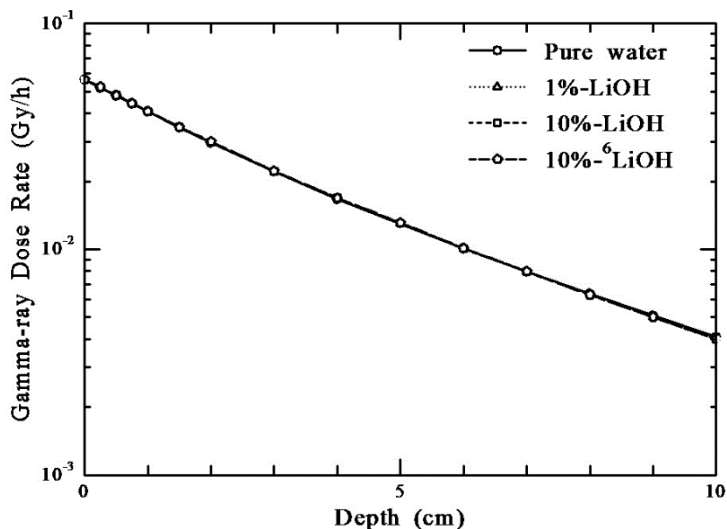
Figure 4 Simulation results for the depth distributions of the fast neutron flux on the central axis in the phantoms.

Figure 4 shows the simulation results for the depth distributions of the fast neutron flux. The statistical errors for all phantoms are contained within the data marks, and the maximum error is 0.3% at the 10 cm depth for the 10%-^{6}LiOH phantom. Figure 5 shows the simulation results for the depth distributions of the primary gamma-ray dose rate. For all phantoms, the statistical errors are largest (0.3%) at the 10 cm depth. As shown in Figures 4 and 5, the depth dose distributions for the fast neutron flux and/or primary gamma-ray dose rate are essentially superimposed across all phantoms. This suggests that fast neutrons and/or primary gamma rays behave the same in water and LiOH-solutions with different Li-6 mixing ratios.

Figure 6 shows the simulation results for the depth distributions of the secondary gamma-ray dose rate. The statistical errors are largest (0.7%) at the 10 cm depth for the 10%-^{6}LiOH phantom. It can be confirmed that the secondary gamma-ray dose rate decreases as the Li-6 concentration increases accordingly with the decrease of thermal neutron flux. Compared with the pure water phantom, the secondary gamma-ray dose rate decreased to 70% for the 1%-LiOH phantom and to 22% for the 10%-LiOH phantom, at the 2 cm depth near the distribution peak. For the 10%-^{6}LiOH

9

phantom, the secondary gamma-ray dose rate was approximately 3.6% and it decreased to almost one twenty-eighth.

210 **Figure 5** Simulation results for the depth distributions of the primary gamma-ray dose rate on the central axis in the phantoms.
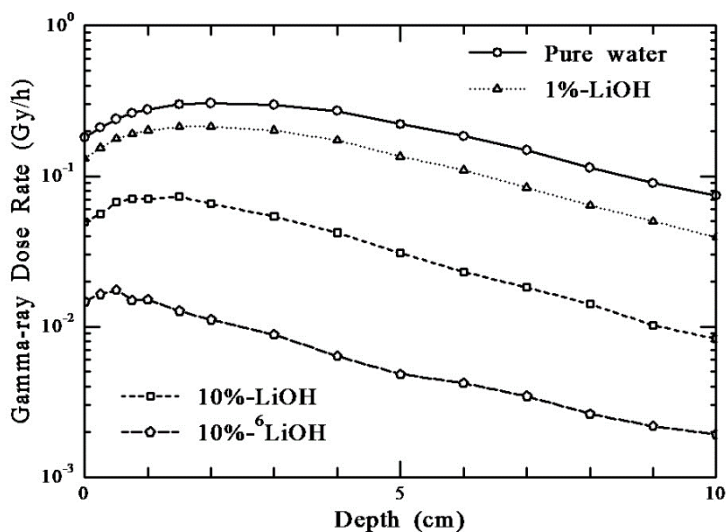

Figure 6 Simulation results for the depth distributions of the secondary gamma-ray dose rate on the central axis in the phantoms.

215

Table 1 Summary of the simulation results at the 2 cm depth for the LiOH concentrations.

LiOH concentration (%)	Li-6 concentration (ppm)	Thermal neutron flux ($cm^{-2}s^{-1}$)	Fast neutron flux ($cm^{-2}s^{-1}$)	Primary gamma-ray dose rate (Gy/h)	Secondary gamma-ray dose rate (Gy/h)
0	0	1.58×10^{8} (100)*	2.02×10^{6} (100)	2.97×10^{-2} (100)	3.05×10^{-1} (100)
0.001	0.26	1.58×10^{8} (100)	2.02×10^{6} (100)	2.97×10^{-2} (100)	3.04×10^{-1} (99.8)
0.01	2.6	1.57×10^{8} (99.4)	2.02×10^{6} (100)	2.99×10^{-2} (101)	3.04×10^{-1} (99.7)
0.1	26	1.53×10^{8} (96.8)	2.01×10^{6} (99.8)	2.98×10^{-2} (100)	2.97×10^{-1} (97.4)
1	260	1.16×10^{8} (73.4)	2.01×10^{6} (99.5)	3.00×10^{-2} (101)	2.13×10^{-1} (69.8)
10	2,600	3.51×10^{7} (22.2)	1.99×10^{6} (98.5)	2.97×10^{-2} (100)	6.55×10^{-2} (21.5)
10#	25,000	3.26×10^{6} (2.1)	1.94×10^{6} (96.0)	2.99×10^{-2} (101)	1.11×10^{-2} (3.6)

* Relative value for the LiOH concentration of 0%, # for 95%-enriched Li-6.

A summary of the simulation results for the LiOH concentrations is shown in Table 1. Values for the thermal neutron flux, fast neutron flux, primary gamma-ray dose rate, and secondary gamma-ray dose rate at the 2 cm depth are included in Table 1. The values in the parentheses are the relative percentage for the LiOH concentration of 0% (pure water phantom). Simulation results demonstrated that the absorbing effect for thermal neutrons occurred when the LiOH concentration was over 1%. The most effective Li-6 concentration was determined to be enriched ^{6}LiOH with a solubility approaching its upper limit. Specifically, simulations indicated that a ^{6}LiOH solution phantom of 10 weight percent is the most effective in enhancing the fast neutron component.

III.B. Experimental measurements

Based on the simulation results, a ^{6}LiOH solution phantom of 10 weight percent was constructed. The measured results for the depth dose distributions of the thermal and fast neutron fluxes on the central axis in the 10%-^{6}LiOH phantom and pure water phantom are shown in Figure 7. Measured values are compared with the simulation results, normalized to the measured results at the peak of the thermal neutron flux for the pure water phantom.
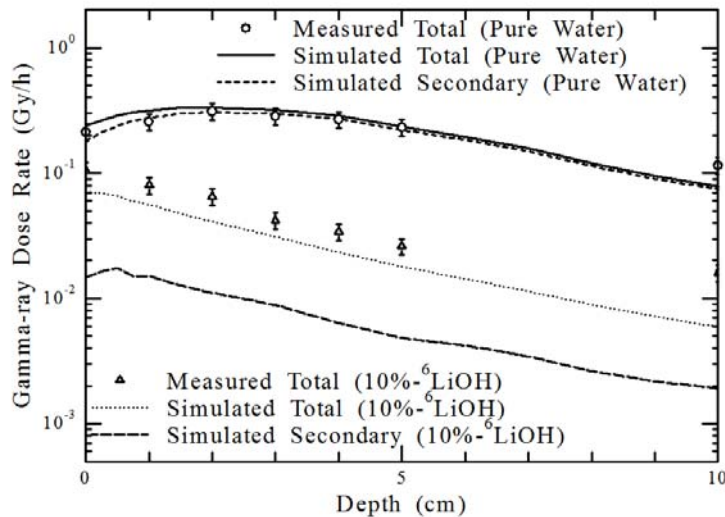
11
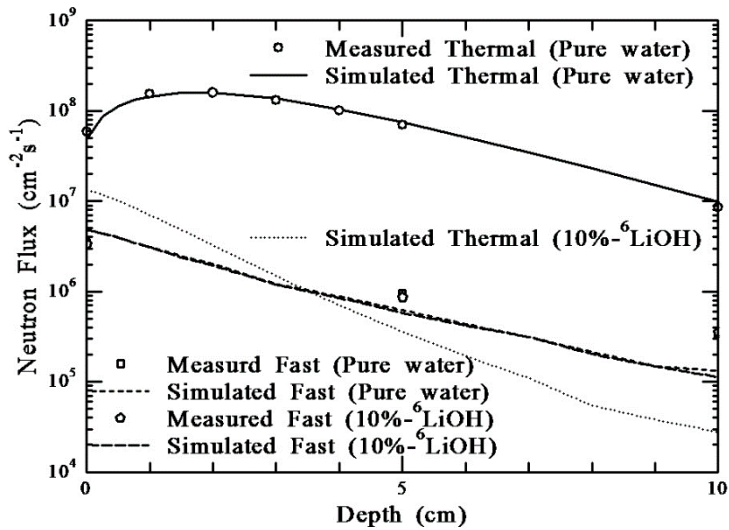
Figure 7 Comparison between the measured and simulation results for the depth distributions of the thermal and fast neutron fluxes in the pure water phantom and the 10%-^{6}LIOH phantom.

For measurements with the 10%-^{6}LiOH phantom, the thermal neutron flux could not be determined because the saturated activity of the cadmium-covered gold wire was almost the same as that of the bare gold wire at each measurement point. The measured results for the fast neutron flux were similar between both phantoms; in agreement with the simulation results. Experimental results confirmed that the thermal neutrons diminished substantially and no decrease in the fast neutrons was observed in the 10%-^{6}LiOH phantom.

For the fast neutron flux distributions, the measured results did not agree with the simulated values. The absolute differences are thought to originate in the beam characteristics at HWNIF owing to the reactor-core conditions of KUR such as the fuel arrangement. The relative differences observed in the distribution curves, are thought to be caused by additional scatter from the irradiation stage and/or irradiation room walls, as these components were not explicitly simulated.

Figure 8 shows a comparison between the measured results and simulation results for the depth distributions of gamma-ray dose rates in the pure water phantom and the 10%-^{6}LIOH phantom. For

the simulation results, the total and secondary gamma-ray dose rate distributions are shown. The data in Figure 8 were normalized in the same manner as described above.

Figure 8 Comparison between the measured and simulation results for the depth distributions of gamma-ray dose rates in the pure water phantom and the 10%-^{6}LIOH phantom.

The gamma-ray dose rate in the 10%-^{6}LiOH phantom decreased to almost one-fifth at a depth of 2 cm, near the distribution peak as compared with the pure water phantom and confirmed with the experimental results. From the simulation results, 70–80% of the gamma rays in the 10%-^{6}LiOH phantom are assumed to be primary gamma rays.

As with the fast neutron flux results, the measured and simulated gamma-ray dose rate distributions were not in agreement. Differences were especially large at depth for the 10%-^{6}LiOH phantom. Similar to the fast neutron flux distributions, it is thought that the absolute differences originated in the beam characteristics for each irradiation condition, and that the relative differences are due to additional scatter contributions not explicitly included in the simulation geometry. It can be postulated that the scatter contributions of the room return components and other equipment are larger in the 10%-^{6}LiOH phantom, in which the generation of the secondary gamma rays is suppressed.

13

IV. DISCUSSION

This study sought to modify the neutron energy spectrum in a phantom containing the appropriate amount of Li-6 resulting in changes to the dose components which could be quantified. Results of this study demonstrated that thermal neutron flux and secondary gamma-ray dose rate diminished substantially but the fast neutron flux and primary gamma-ray dose rates were hardly affected in the phantom using 10%-^{6}LiOH solution. The 10%-^{6}LiOH phantom was nearly one-fiftieth as sensitive to thermal neutrons and one-fifth as sensitive to gamma rays, as compared with the pure water phantom. Based on these results, the effectiveness for the relative enhancement of the fast neutron dose in the phantom using the 10%-^{6}LiOH solution, was estimated. The effectiveness of the dual phantom technique using the combination of a pure water phantom and a 10%-^{6}LiOH phantom, was considered.

For the neutron flux distributions in the pure water phantom and the 10%-^{6}LiOH phantom, the calculated thermal and fast neutron fluxes were converted into absorbed dose rates in normal tissue.[13] The composition for normal tissue was assumed to be H:11.1, C:12.7, N:2.0, O:74.2 in weight percent,[14] and the density was assumed to be 1.0 g/cm^3. Figures 7 and 8 show the depth distributions of the total dose rate and its breakdown in the pure water phantom and the 10%-^{6}LiOH phantom, respectively.

In the pure water phantom, the breakdown of the total dose rate at a depth of 2 cm near the distribution peak is 12% for fast neutrons, 15% for thermal neutrons, and 73% for gamma rays, as shown in Figure 9. This breakdown changes to 6% for fast neutrons, 12% for thermal neutrons, and 82% for gamma rays at a depth of 5 cm, and further changes to 4% for fast neutrons, 5% for thermal neutrons, and 91% for gamma rays at a depth of 10 cm. Over the interior of the phantom, the contribution of gamma rays is dominant and becomes larger at depth.

In the 10%-^{6}LiOH phantom, the breakdown of the total dose rate at a depth of 2 cm is 56% for fast neutrons, 2% for thermal neutrons, and 42% for gamma rays, as shown in Figure 10. This breakdown changes to 47.5% for fast neutrons, 0.5% for thermal neutrons, and 52% for gamma rays

14

at a depth of 5 cm, and further changes to 34.9% for fast neutrons, 0.1% for thermal neutrons, and 65% for gamma rays at a depth of 10 cm. In the 10%-^{6}LiOH phantom, the thermal neutron dose rate decreases to below almost one-thirtieth of the fast neutron dose rate. The gamma-ray dose rate decreases to an equilibrium with the fast neutron dose rate at a depth of 4 cm. At depths greater than 4 cm the gamma-ray dose rate remains larger than the fast neutron dose rate and is approximately 2.5 times larger at a depth of 10 cm.
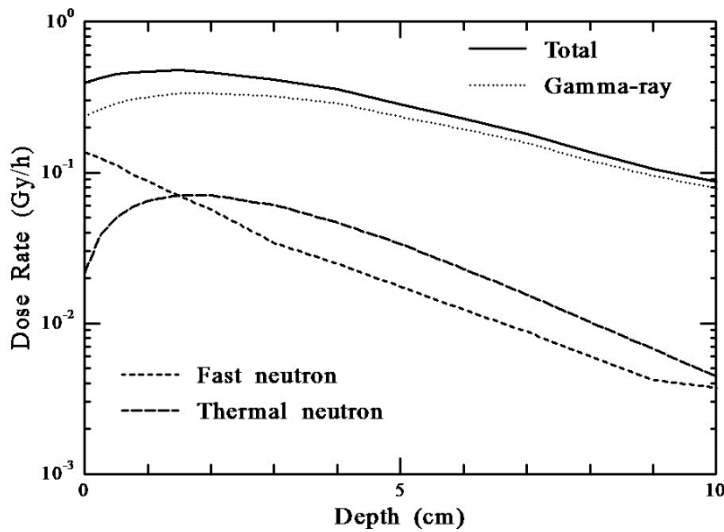

Figure 9 Depth distributions of the total dose rate and breakdown in the pure water phantom.
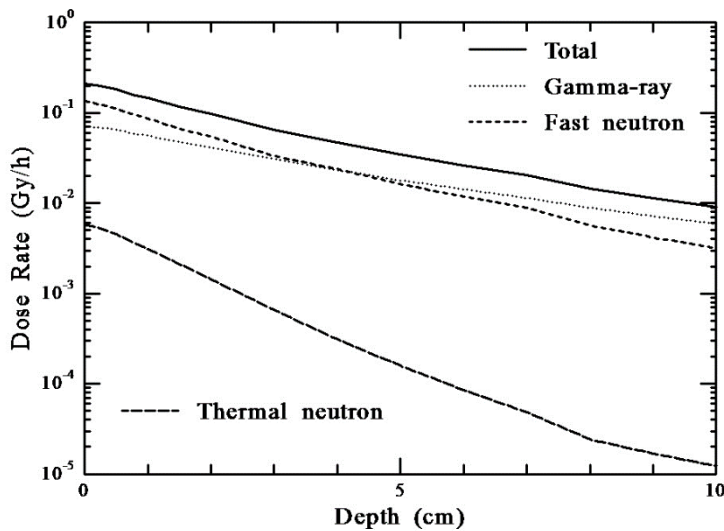

Figure 10 Depth distributions of the total dose rate and breakdown in the 10%-^{6}LiOH phantom.

15

From the results, a larger contribution of fast neutron dose is realized with the 10%-^{6}LiOH phantom. The accuracy of dose measurements for the fast neutron component in biological experiments may improve by using the dual phantom technique employing the 10%-^{6}LiOH

310 phantom in which the contribution of fast neutron dose is approximately 50% greater, and the pure water phantom in which the fast neutron dose contribution is at most 10%.

V. CONCLUSION

A dual-phantom technique was developed to improve the accuracy of the dose measurement for

315 fast the neutron component incident in a BNCT irradiation field. This study modified the neutron energy spectrum in a phantom, resulting in a different breakdown of dose components by using a phantom containing an appropriate quantity of Li-6.

For the LiOH phantom, it was found that the absorbing effect for thermal neutrons became apparent when the LiOH concentration was over 1%, based on the simulation results of the Li-6

320 mixing ratio in a LiOH solution. The most effective Li-6 concentration was determined to be enriched ^{6}LiOH with a solubility approaching its upper limit. In this work, a ^{6}LiOH of 95%-enriched Li-6, which was in stock at KURRI, was used to prepare the water solution of 10 weight percent for use in the phantom.

Using the prepared 10%-^{6}LiOH phantom, it was experimentally confirmed that thermal neutron

325 flux and secondary gamma-ray dose rate diminished substantially but the fast neutron flux and primary gamma-ray dose rates were minimally affected. The contribution of the fast neutron dose was improved to almost 50% on the central axis in the 10%-^{6}LiOH phantom, while the fast neutron dose contribution was at most 10% in the pure water phantom. Applying the dual phantom technique using the combination of a pure water phantom and a 10%-^{6}LiOH phantom may improve

330 the accuracy of dose measurement for fast neutron components in biological experiments.

Future work includes biological experiments for RBE estimation for fast neutron components incident in the epi-thermal neutron beams from the BNCT irradiation systems such as KUR-HWNIF or C-BENS. As shown by Tanaka *et al*[4], the neutron energy spectra of the obtained epi-thermal neutron beams are remarkably different between KUR-HWNIF and C-BENS. The

335 difference in energy spectra is likely reflected in the RBEs and should be considered during experimental measurements. Unfortunately, enriched ^{6}LiOH is expensive and difficult to obtain. Future studies will seek to develop a phantom containing lower-enriched Li-6 or natural Li. For example, LiF can be loaded to nearly 50% when polyethylene is used as a base material. We are also planning to prepare a solid LiF polyethylene phantom for the study of RBE.

340

345 **References**

[1]G. L. Locher, ''Biological effects of therapeutic possibilities of neutrons,'' Am. J. Roentgenol. **36**, 1–13 (1936).

[2]Y. Sakurai and T. Kobayashi, "Characteristics of the KUR Heavy Water Neutron Irradiation Facility as a neutron irradiation field with variable energy spectra," Nucl. Instr. Meth. A **453**, 569-

350 596 (2000).

[3]X. Shen, K. Nakajima, H. Unesaki and K. Mishima, "Reactivity insertion transient analysis for KUR low-enriched uranium silicide fuel core", Ann. Nucl. Energy **62**, 195-207 (2013).

[4]H. Tanaka, Y. Sakurai, M. Suzuki, S. Masunaga, Y. Kinashi, G. Kashino, Y. Liu, T. Mitsumoto, S. Yajima, H. Tsutsui, A. Maruhashi and K. Ono, "Characteristics comparison between a

355 cyclotron-based neutron source and KUR-HWNIF for boron neutron capture therapy," Nucl. Instr. Meth. B **267**, 1970-1977 (2009).

17

[5]C. N. Culbertson, S. Green, A. J. Mason, D. Picton, G. Baugh, R. P. Hugtenburg, Z. Yin, M. C. Scott, and J. M. Nelson, "In-phantom characterisation studies at the Birmingham Accelerator-Generated epIthermal Neutron Source (BAGINS) BNCT facility", Appl. Radiat. Isot. **61**, 733-738 (2004).

[6]C. Ceballos, J. Esposito, S. Agosteo, P. Colautti, V. Conte, D. Moro and A. Pola, "Towards the final BSA modeling for the accelerator-driven BNCT facility at INFN LNL", Appl. Radiat. Isot. **69**, 1660-1663 (2011).

[7]A. J. Kreiner, W. Castell, H. Di Paolo, M. Baldo, J. Bergueiro, A. A. Burlon, D. Cartelli, V. Thatar Vento, J. M. Kesque, J. Erhardt, J. C. Ilardo, A. A. Valda, M. E. Debray, H. R. Somacal, J. C. Suarez Sandin, M. Igarzabal, H. Huck, L. Estrada, M. Repetto, M. Obligado, J. Padulo, D. M. Minsky, M. Herrera, S. J. Gonzalez and M. E. Capoulat, "Development of a Tandem-Electrostatic-Quadrupole facility for Accelerator-Based Boron Neutron Capture Therapy", Appl. Radiat. Isot. **69**, 1672-1675 (2011).

[8]H. Kumada, A. Matsumura, H. Sakurai, T. Sakae, M. Yoshioka, H. Kobayashi, H. Matsumoto, Y. Kiyanagi, T. Shibata and H. Nakashima, "Project for the development of the linac based NCT facility in University of Tsukuba", Appl. Radiat. Isot. **88**, 211-215 (2014).

[9]A. J. Kreiner, M. Baldo, J. R. Bergueiro, D. Cartelli, W. Castell, V. Thatar Vento, J. Gomez Asoia, D. Mercuri, J. Padulo, J. C. Suarez Sandin, J. Erhardt, J. M. Kesque, A. A. Valda, M. E. Debray, H. R. Somacal, M. Igarzabal, D. M. Minsky, M. S. Herrera, M. E. Capoulat, S. J. Gonzalez, M. F. del Grosso, L. Gagetti, M. Suarez Anzorena, M. Gun and O. Carranza, "Accelerator-based BNCT", Appl. Radiat. Isot. **88**, 185-189 (2014).

[10]International Atomic Energy Agency, "Current status of neutron capture therapy", IAEA-TECDOC-1223, 2001.

[11]Y. Sakurai, T. Fujii, H. Tanaka, M. Suzuki, Y. Liu, G. Kashino, Y. Kinashi, S. Masunaga, K. Ono and A. Maruhashi, "A study on QA-phantom for boron neutron capture therapy",

Proceedings of the 14th International Congress on Neutron Capture Therapy, Comision Nacional de Energia Atomica, 2010, pp. 254-256.

[12]J. F. Briesmeister, "MCNP-a general Monte Carlo n-particle transport code, version 4C," LA-**13709**-M (2000).

[13]R. S. Caswell, J. J. Coyne and M. L. Randolph, "Kerma factors for neutron energies below 30 MeV," Radiat. Res. **83**, 217-254 (1980).

[14]W. S.Synder, M. J. Cook, E. S. Nasset, L. R. Kahrhausen, G. P. Howells and L. H. Tipon, *Report of the Task Group on Reference Man* (Pergamon Press, Oxford, 1975).

390